ELSEVIER

Contents lists available at ScienceDirect

Nuclear Inst. and Methods in Physics Research, A

journal homepage: www.elsevier.com/locate/nima



Understanding the enhancement of scintillation light in xenon-doped liquid argon



D.E. Fields a, R. Gibbons a,1, M. Gold a,*, N. McFadden a, S.R. Elliott b, R. Massarczyk b

- ^a Department of Physics and Astronomy, MSC07 4220, 1 University of New Mexico, Albuquerque NM 87131-0001, USA
- ^b Physics Division, Los Alamos National Laboratory MS H803, P-23, Los Alamos, NM, 87545, USA

ARTICLE INFO

Keywords: Liquid argon Scintillation Xenon doping

ABSTRACT

Measuring the scintillation light in noble gases is an important detection technique in particle physics. Numerous rare event searches like neutrino beam experiments, neutrino-less double beta-decay, and dark matter searches use argon-based detectors. In liquid argon, the light yield can be enhanced by the addition of a small quantity of xenon, where $\sim 10-1000$ ppm are added. The general enhancement mechanism and its pathway via an energy transfer between argon and xenon excimers is well known, however the importance of absorption of argon excimer emission by atomic xenon has not been fully appreciated. This absorption significantly reduces the light yield in commercially available argon (extracted from air) which contains trace amounts (~ 0.1 ppm) of xenon. The addition of a small xenon dopant of ~ 10 ppm recovers this lost light resulting in an increased light yield over un-doped argon of about a factor of two. In this paper we introduce a model for the light production in xenon doped argon, including absorption and re-emission, and compare it to the measured time dependence of light emission in xenon-doped argon.

1. Introduction

The use of liquid noble gases in detectors in physics experiments has become a mainstay. In particular, liquid argon (LAr) has become widely used because of its low cost. A number of experiments use scintillation light in low rate, large volume/mass applications needed in dark sector searches [1-3] or neutrino detection [4], or as active shield detector for neutrino-less double beta decay experiments like GERDA [5] or LEGEND [6]. Due to the short wavelength of the argon scintillation light (128 nm) and the low sensitivity of common light detectors at this range, LAr experiments generally require the use of a wavelength shifting material. Common materials like Tetraphenyl Butadiene, (TPB), have to be coated on detectors, light guides, or on the walls of the cryostats. The possibility of shifting the light within the LAr itself to a different wavelength is therefore intriguing. One possibility is the doping of LAr with xenon with the subsequent creation of xenon excimers which emit light at higher wavelength (175 nm) [7]. Previous works have demonstrated that a small dopant concentration of ~ 10 ppm is sufficient to transfer a large portion of the argon scintillation to the xenon emission wavelength [8,9].

When energy is deposited in pure LAr, argon excimers form which emit light at 128 nm. It is known that trace amounts (\sim 0.1 ppm) of xenon remain in commercially available argon extracted from air, leading to absorption of the argon excimer light [10]. In this paper we

present a model for this absorption that agrees with our measurement of the light emission as a function of time. This model explains changes in light yield as a function of xenon concentration in the LAr.

2. Light emission in xenon-doped argon

The existence of trapped exciton states of xenon in liquid argon was discovered by Raz and Jortner [11]. These states were observed in the absorption spectrum of liquid argon with $\sim\!0.1$ ppm xenon [10]. The measured absorption of light through a path length of 11.6 cm liquid argon is shown in Fig. 1 together with the 128 nm argon excimer emission line superimposed.

This absorption spectrum is convoluted with the argon excimer emission to obtain the results seen in Fig. 2, where it is clear that even at low levels of xenon (0.1 ppm) and relatively short distances (11.6 cm), more than half of the initial 128 nm light is absorbed.

These curves are then integrated over wavelength to obtain the transmission as a function of distance shown in Fig. 3. This transmission curve is then fitted to the double exponential:

$$T = Ae^{-x/\lambda_1} + (1 - A)e^{-x/\lambda_2}. (1)$$

From the fit, for distances in the range from 10–100 cm, the effect is to absorb an approximately constant factor of A=0.62 of the total

^{*} Corresponding author.

E-mail address: mgold@unm.edu (M. Gold).

¹ currently at Physics Department, Bldg. 50, Lawrence Berkeley National Laboratory, Berkeley, CA, 94720-50, USA.

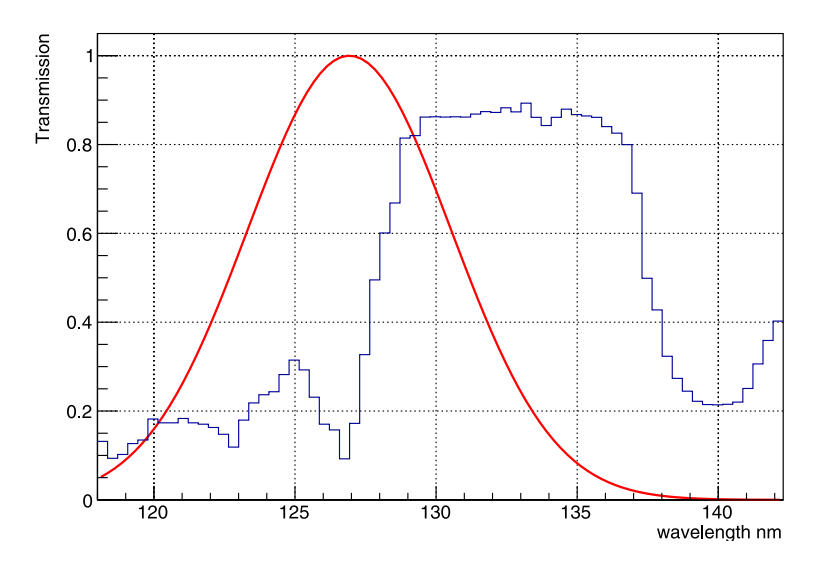


Fig. 1. Transmission of light as a function of wavelength through 11.6 cm path of liquid argon with 0.1 ppm xenon [10]. Superimposed (red line) is the argon excimer 128 nm emission line.

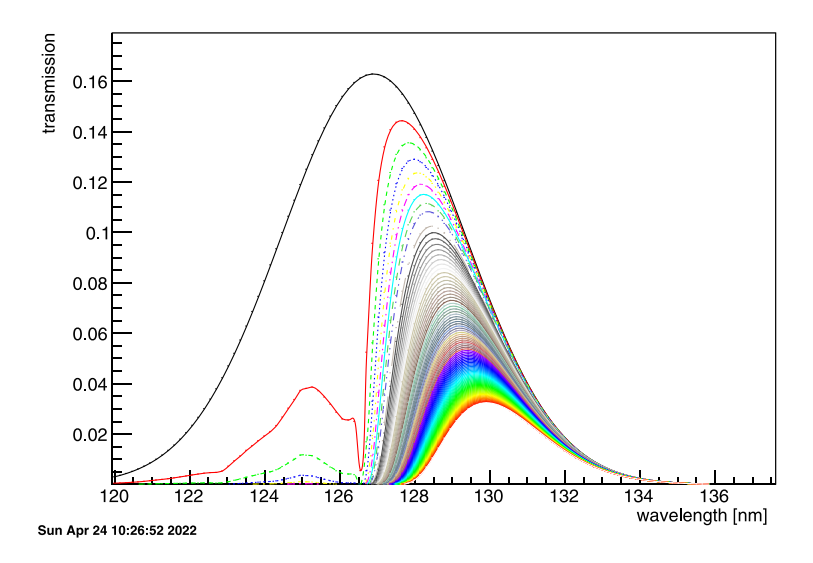


Fig. 2. Results of the convolution of the two graphs of Fig. 1. Each curve is an additional step of 11.6 cm (the initial path length) over 100 steps with a maximum distance of 1160 cm.

light, taken from the fit values. This is a key parameter in our model. The cross section for this absorption in liquid argon can be written as $\sigma_{abs}=1/nl_{abs}c$, where n is the atomic number density of liquid argon $(2.1\times10^{28}/\text{m}^3)$, l_{abs} is the effective absorption length from the fit (12.7 cm, see fit value of λ_1 in Fig. 3), and c is the concentration of xenon atoms in parts per million (0.1 ppm, as given in the reference for the xenon concentration for their data). The result is $\sigma_{abs}=37.5\text{Mb}$, in agreement with the result of Ref. [12]. It should be noted that the horizontal axis of the curve (and thus the fit parameters λ_1 and λ_2) of Fig. 3 can be scaled for different xenon concentrations by the factor (xenon concentration in ppm)/(0.1 ppm).

Argon excimers Ar_2^* are created in singlet (S) or triplet (T) states with about 85% in the T state for gammas [13]. The argon excimer singlet S has a lifetime of 5 ns, whereas the triplet T has a much longer lifetime of ~ 1600 ns. As these excimers decay, xenon atoms absorb light and form an exciton state. This state immediately forms the mixed state

ArXe*[14] excimer. The lifetime of the mixed state is long, 4700 ns, and has a decay wavelength of 150 nm [15]. There is a competing process of collisional quenching of the excimer states at a rate of about $1/(7.7 \mu s)[16]$ that contributes to total light loss. The mixed state can form a xenon excimer Xe_2^* through diffusion to xenon at a rate which increases with the xenon dopant.

Our model consists of four coupled differential equations for the number of molecules as a function of time t for the excimer states argon singlet S(t), argon triplet T(t), and the combined singlet and triplet states of the mixed M(t) and xenon X(t):

$$\dot{S} = -S/\tau_S - (k_x + k_q) S \equiv -\lambda_1 S \tag{2}$$

$$\dot{T} = -T/\tau_T - \left(k_x + k_q\right)T \equiv -\lambda_3 T \tag{3}$$

$$\dot{M} = -\left(1/\tau_M + k_x + k_q'\right)M + \left(k_x + A/\tau_S\right)S + \left(k_x + A/\tau_T\right)T\tag{4}$$

$$\dot{X} = -X/\tau_{x} + k_{x}M\tag{5}$$

² The ratio of singlet to triplet states depends on the type of ionizing radiation, presence of an electric field, etc.

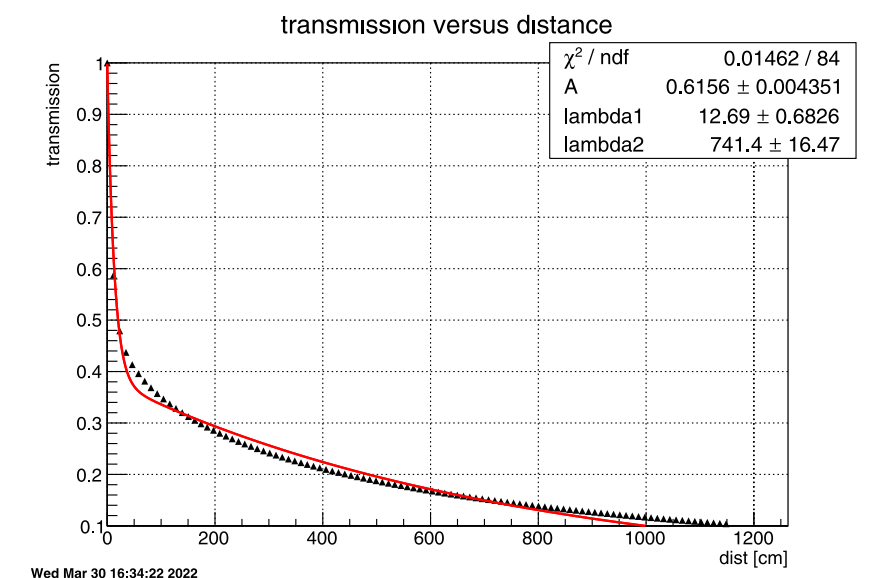


Fig. 3. Transmission of argon 128 nm light with distance from convolution of argon emission spectrum with transmission data of Fig. 1. The red curve is a double exponential fit to the data.

In these equations, the lifetimes of the different states are labeled using τ in combination with the corresponding letter as index. We introduce collisional de-excitation factors due to quenching $k_q=1.3\times 10^{-4}~{\rm ns}^{-1}$, and $k_q'\sim k_q$, as used in Ref. [16], although we note that the collisional quenching may be stronger for the more weakly bound M and X excimers.

We use $k_x=2.9\times10^{-4}~[ppm]~ns^{-1}[17].^3$ The absorption of the argon excimer de-excitation light at 128 nm is parameterized by the dimensionless constant A which we take from the fit in Fig. 3. Although this number varies with dopant, especially at dopant levels less than 1 ppm, it is unknown what the xenon concentration was in the undoped LAr of our experiment, therefore we use the same absorption across all data sets.

Integrating these equations, the total emitted light yield $\ell(t)$ as a function of time is given by,

$$\ell(t) = N_1 (1-A) e^{-t\lambda_1} / \tau_S + N_3 (1-A) e^{-t\lambda_3} / \tau_T + M(t) / \tau_M + X(t) / \tau_X \end{(6)}$$

where N_1 and N_3 are the number of initial singlet and triplet states, respectively. The decay constants are defined using the introduced half-lives τ : $\lambda_X = 1/\tau_X$, $k_x' = 1/\tau_M + k_x + k_q'$, $C_1 = k_x + A/\tau_S$, $C_3 = k_x + A/\tau_T$. The total number of mixed states as a function of time $M(t) = M_1(t) + M_3(t)$ is

$$M_i(t) = \frac{N_i C_i}{\lambda_i - k_x'} \left[e^{-tk_x'} - e^{-t\lambda_i} \right]$$
 (7)

for i = 1, 3.

Similarly, the number of xenon states can be described as $X(t) = X_1(t) + X_3(t)$ with

$$X_{i}(t) = \frac{N_{i}C_{i}k_{x}}{\lambda_{i} - k_{x}'} \left[\frac{e^{-tk_{x}'} - e^{-t\lambda_{x}}}{\lambda_{x} - k_{x}'} - \frac{e^{-t\lambda_{i}} - e^{-t\lambda_{x}}}{\lambda_{x} - \lambda_{i}} \right], \tag{8}$$

again for i=1,3. When fitting this distribution to the data, one has to consider that the timing resolution of our detector smears out the exact distributions. We used the measured rise time of the singlet light emission (see Fig. 8 to determine the timing resolution of our setup, and fold this as a Gaussian distribution into the exponential decay.

3. Experimental setup

The liquid argon test stand at UNM is described in detail in Ref. [9]. The same reference shows that the measured properties of the argon are in good agreement with previous measurements, and that the doping system is well understood. The apparatus is a 100L cylindrical liquid argon cryostat with a single PMT mounted on the bottom facing upwards. The 3" Hamamatsu R11065 Photomultiplier (PMT) has a TPB coated acrylic disk fixed to the front of the tube to shift the light to a wavelength with good detection efficiency.⁴ The cryostat was filled with argon gas and liquefied using a CryoMech cold head. The amount of LAr in the cryostat was monitored by constantly measuring the weight of the cryostat. On top of the liquid phase, a gas phase is present due to boil-off. The argon gas was circulated through a SAES PS4-MT3/15-R getter, which purifies noble gasses to less than 1 PPB of: H₂O, CO, CO₂, N₂, H₂, CH₄ prior to liquefaction [20]. The operation of the getter and the doping system was verified previously with the introduction of a known amount of nitrogen and monitoring the light yield initially decreasing and then recovering [9]. For the data sets presented in this work, xenon dopant was added to achieve the four concentrations of 1.00 ± 0.06 ppm, 2.0 ± 0.1 ppm, 5.0 ± 0.3 ppm, and 10.0 ± 0.5 ppm. The concentration of the xenon is determined from the volume and pressure of xenon added, and the measured weight of liquid argon in the cryostat. The increase in uncertainty with dopant level is an accumulation of uncertainties in dopant as more xenon was added. Including the un-doped data then, we have a total of five data sets (referred to as sets 0, 1, 2, 3, and 4 for the un-doped, 1 ppm, 2 ppm, 5 ppm, and 10 ppm respectively).

Some data was taken in coincidence with scintillator paddles located above and below the cryostat as a cosmic trigger, however, all data presented here was self-triggered data. Therefore, the events were caused by a mixture of cosmogenics and radiogenics.

4. Event selection and data set preparation

We modified the analysis algorithm used in Ref. [9] due to concerns about after-pulsing in the PMT as well as concerns about the pulsefinding efficiency immediately following the large singlet pulse due to

 $^{^3}$ This number appears without reference in [12]. It is close to the value of $k_x=2.4\times 10^{-4}~[ppm]~ns^{-1}$ calculated from the diffusion limited reaction rate using Van der Walls values for the atomic radii [18].

 $^{^4}$ It should be noted here that the wavelength dependence of TPB is essentially flat over the region 120--200 nm [19], so no additional correction is needed for this study.

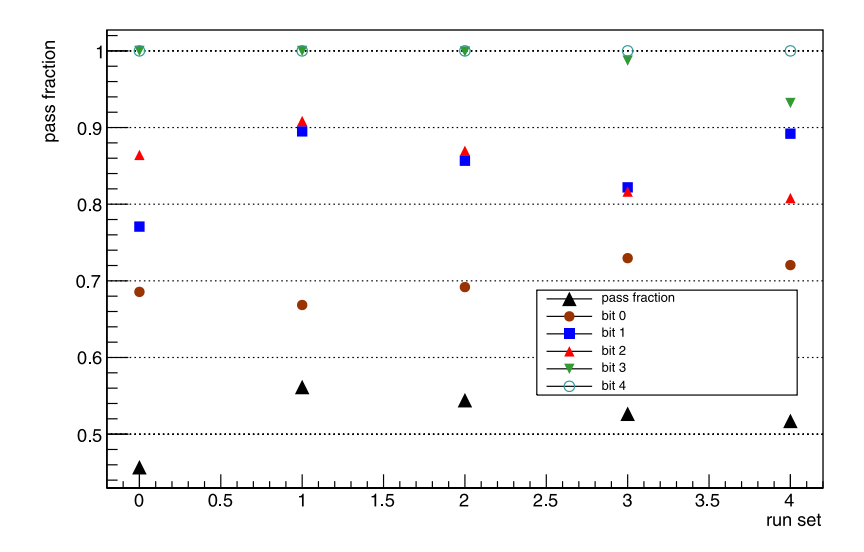


Fig. 4. Event clean-up cuts for each data set with cut bits are defined in the text. The sets 0-4 correspond to the doping by 0, 1, 2, 5, and 10 ppm xenon.

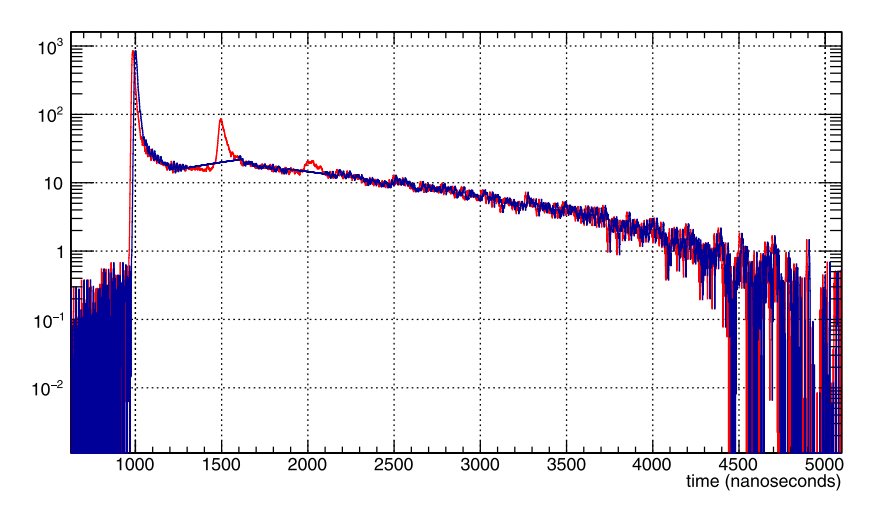


Fig. 5. Typical time distribution in an event showing PMT after-pulsing (red). In this case, the event is from the un-doped data set. Each event has the after-pulsing removed by interpolation (blue). The peak time for each event is also shifted to align at 1000 ns.

overshoot in the AC coupled PMT (a remnant of this overshoot can be seen in the first two data sets, see Fig. 7). The previous analysis used a derivative-based pulse-finding algorithm. The new algorithm simply sums the event waveforms by run. Additionally, we removed events using data clean-up cuts described below. Because we do not do pulse finding, we are unable to recover the small signal above the noise for late (>3000 ns) times.

During data taking, individual 10 μs long waveforms are recorded. The data includes 1 μs prior to the trigger from which a baseline is determined. We used a threshold trigger tuned to $\sim\!\!15$ PE. This value was estimated by comparing the singlet peak of the waveforms to the individual small amplitude pulses in the late light. This threshold was introduced to reduce noise triggers while still remaining very efficient for ionization events. With this threshold, our data was virtually all due to cosmic rays. However, it should be noted for later reference that triggered events represent ionizing events from all orientations and distances to the PMT, and because of the effects of xenon doping, the subset of these cosmic rays may differ between dopant sets.

A series of cuts was applied to remove saturated and pile-up events (labeled as bits 0–4 in Fig. 4). Saturated events, which come from high energy cosmic ray events, create a false singlet to non-singlet light ratio

and are removed (bit 0). Individual waveforms which show either a pulse before the singlet peak (bit 1) or mismatch in baselines at the beginning and the end of the event (bit 2) are also removed from the data set. These cases do not allow for a correct estimate of the singlet value due to a disturbed baseline. Pile-up events and events with high noise can be identified by the presence of a second large peak after the singlet (bit 3). Fig. 4 shows the overall acceptance is \sim 55% and approximately constant across dopant sets. Individual waveforms have their baseline subtracted, and the peak of the singlet is aligned to $t=1000\,\mathrm{ns}$ to avoid additional smearing due to these time offsets. Additionally, a PMT after-pulsing artifact (due to presence of helium in the PMT) is removed by a simple linear interpolation algorithm (see Fig. 5.) All events which pass the data quality cuts are then summed by run.

The integrated light from the singlet peak (900–1020 ns) and the late light region (1020–2030 ns) is shown run-by-run in Fig. 6. The late light region is defined to avoid late-time baseline shifts that we do not attempt to correct (see Fig. 7). A step-wise increase in the late light region with dopant is clearly apparent, with sets corresponding to 0, 1, 2, 5 and 10 ppm, whereas the singlet light changes very little with dopant (see Fig. 8). A few runs have lower yields than the majority

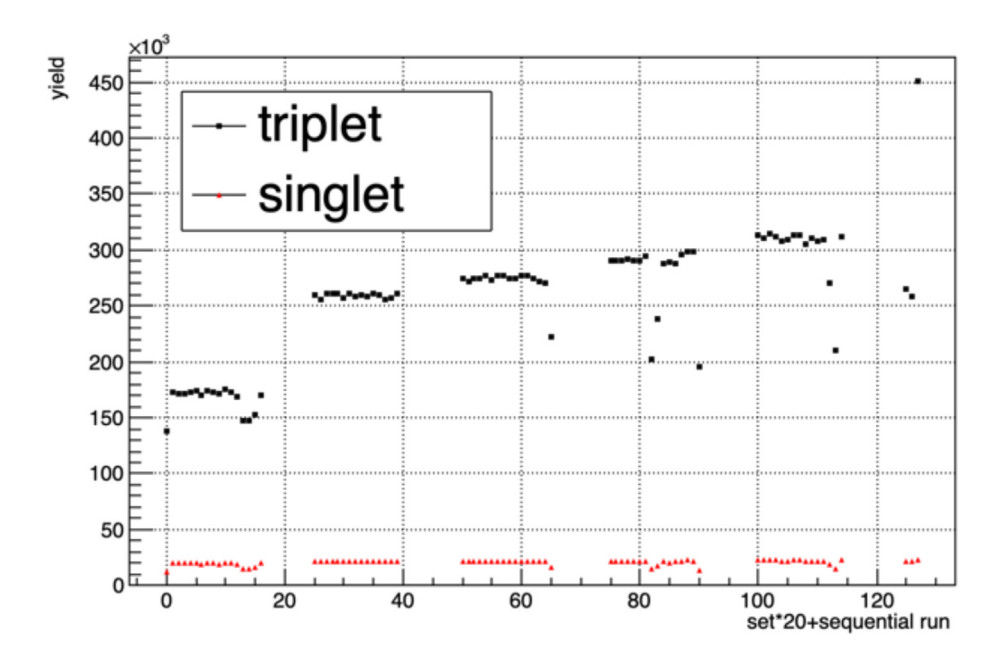


Fig. 6. Relative light yield in the singlet (summed from 900 to 1020 ns) and triplet region (summed from 1020 to 2300 ns) by run number to monitor the stability of the doping.

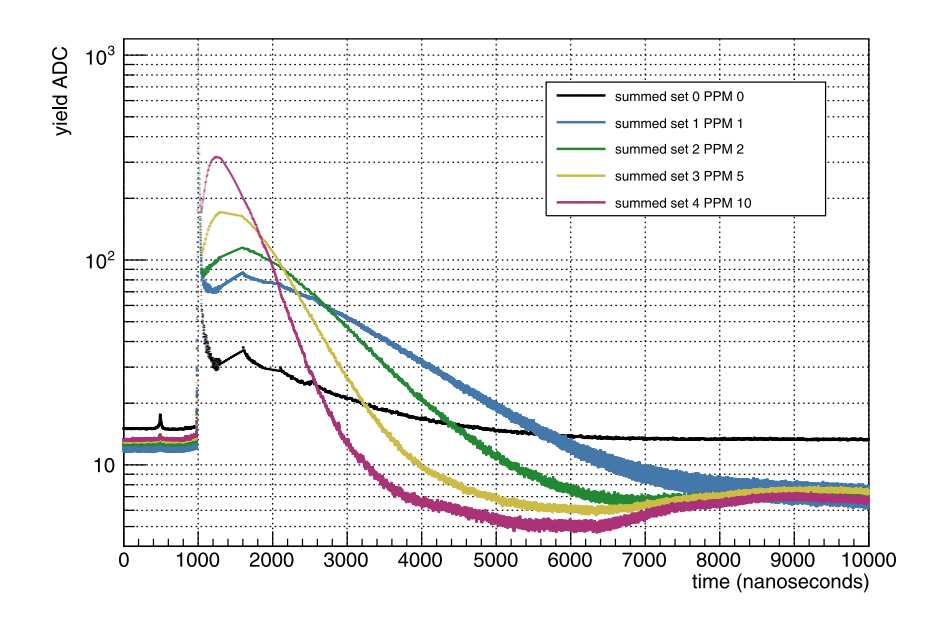


Fig. 7. Summed time distributions of the individual events as a function of doping level (0, 1, 2, 5, and 10). The baselines before the singlet peak are all centered around zero in the data, but a small offset has been added in order to plot the data on a log scale.

within a set, and while we do not yet understand the low yield for these runs, they were clearly anomalous and inconsistent with each other hence they were removed from further analysis. The waveforms are then summed by dopant sets and normalized to the number of events in each set (See Fig. 7).

The number of generated Cherenkov photons above 120 nm in LAr is about 700 per cm, so this could constitute some portion of the "singlet peak". However, we cut events that saturated the PMT which would be expected from events where the track points towards the PMT, and is also where the Cerenkov photons would be dominant. Additionally, in our previous paper [9], we compared our data to a full GEANT simulation (without Cherenkov) and saw good agreement

with our data (see also [21], for example figure 7.7). Our assumption in this paper is that Cherenkov light plays a minor role, and is certainly not important to the main thrust of the paper — the changing time distribution of the light yield with xenon doping.

In total about 400,000 events for each doping set allow an analysis of the light time distribution with negligible statistical uncertainty. The increase of light with dopant as well as the shift of the light to earlier times is apparent in the integral waveforms shown in Fig. 9.

5. Model fitting results

The time distribution of detected light from each set are fitted with the model for each level of doping with only two free parameters for

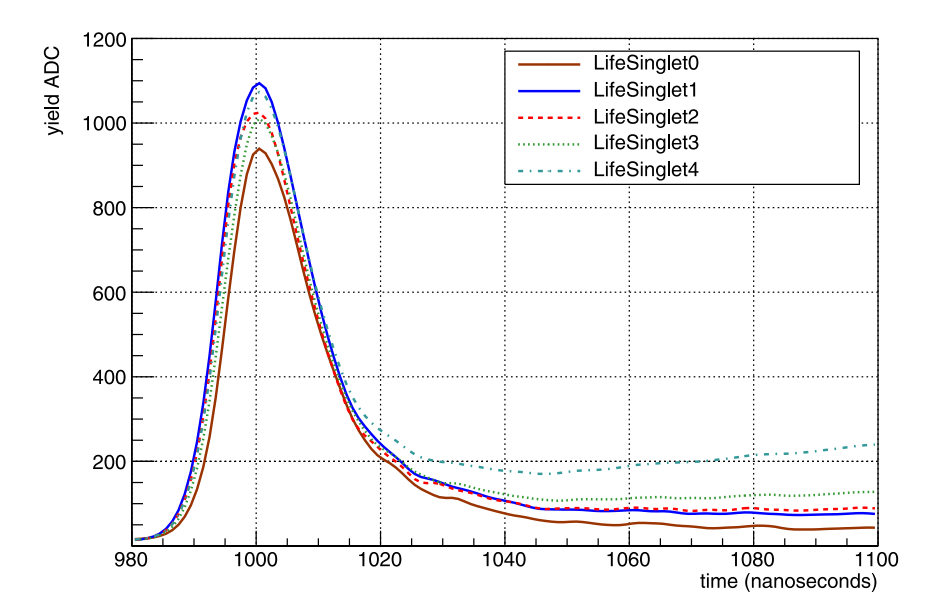


Fig. 8. Zoom in into the singlet region of Fig. 7 with the same color coding. The rise time of the singlet peak (approximately 6 ns) was used to determine the timing resolution of the setup.

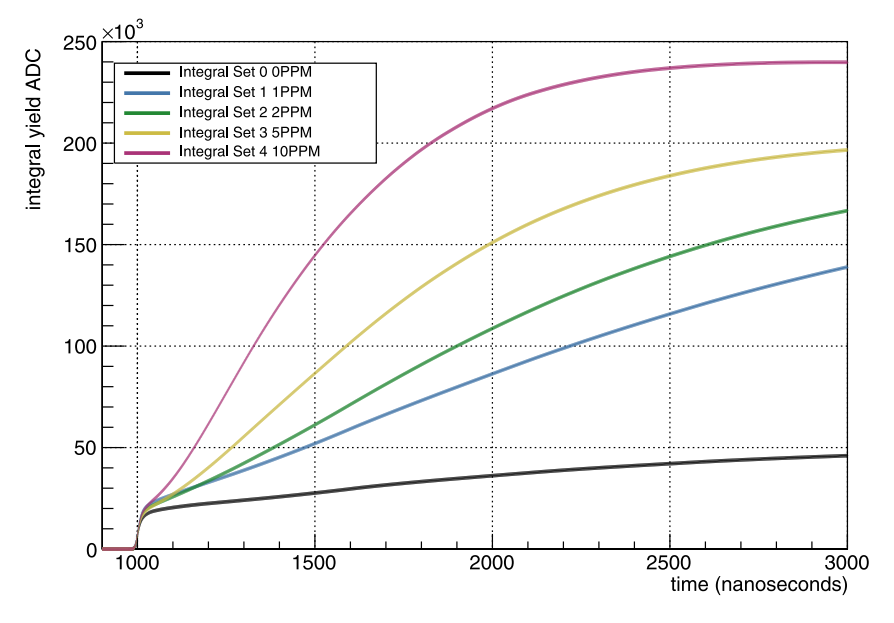


Fig. 9. Integrated time distributions of Fig. 7 (1000 to 3000 ns) for each with doping level 0, 1, 2, 5, and 10. The shift in the light to early times as well as the increase in light with dopant is apparent.

each data set — the normalization (norm) and the fraction of singlet to triplet states (sfrac). The fit region was limited to the region between the trigger time of 980 ns and 3000 ns to avoid problems with the baseline and since the biggest impact of doping is seen in this region. Since we do not have a measurement of the residual xenon in our undoped argon, we fit by hand the xenon concentration for that set, and used the resulting value (0.4 ppm) as an offset for the remaining sets. With this offset, the constant value of absorption, A=0.62, used for all data sets is justified. The fits are shown in Fig. 10. All curves show good agreement with the measured light distribution in each data set.

The normalization can be thought of as the total number of initial singlet plus triplet argon excimers (after correction for acceptance and efficiency), and should not depend on doping levels. However, since the absorption of the 128 nm light can affect the trigger bias, the relatively small variations seen in the normalization are not considered significant.

6. Discussion

We can use our model to predict the light produced by the separate excimers as a function of dopant. These curves are shown in Figs. 11 and 12, which shows the time-integrated light yield of the individual components as a function of doping. If the absorption is set to zero (Fig. 11) the results are in good agreement with the model by Segreto [13] which indicates a 20% increase in total light yield

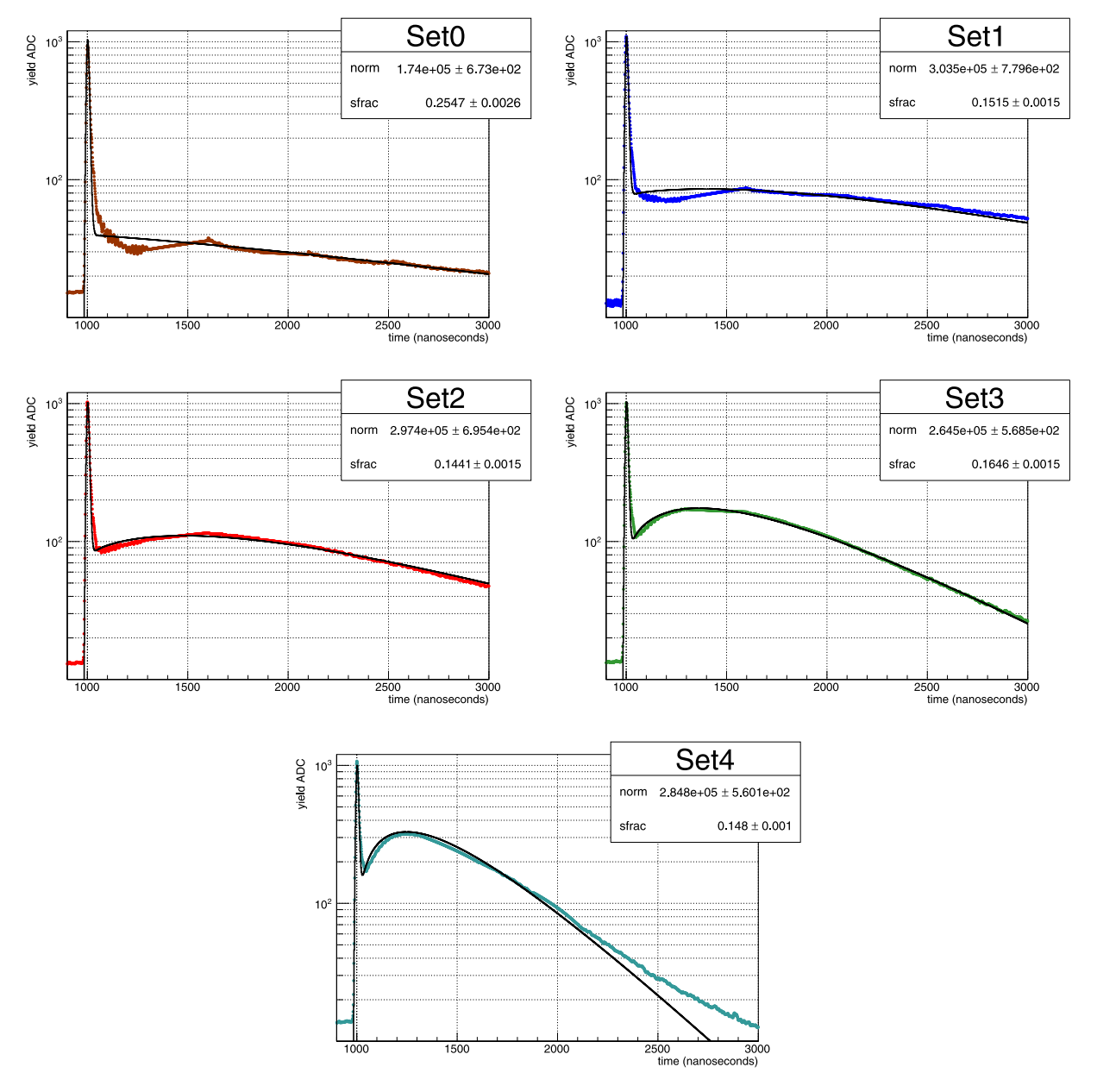


Fig. 10. Fits to the different doping data sets. The solid curve fits are the model with just two fit parameters (norm and sfrac, as described in the text). The xenon concentrations are shifted by 0.4 relative to the added xenon, representing the residual xenon in our (commercially available, extracted from air) argon, and has a better fit to the undoped data.

from 0 ppm to 100 ppm xenon concentration, where we see a 15% increase from 0.1 ppm to 100 ppm without absorption. In our model (without absorption) this increase is due to the transfer of the argon excimer state to the mixed state with dopant, a process which competes with the quenching of the argon state. However, the model of that reference does not include absorption by atomic xenon which increases the rate of mixed state formation. Furthermore, that model does not include quenching of the mixed state. With the inclusion of absorption (Fig. 12), results from our data and the results from Ref. [10] are well described. The light yield without dopant is greatly suppressed by the large absorption and creation of mixed excimers with a long lifetime. Both the triplet excimers and the mixed excimers are quenched with the result that much of the light is lost. Addition of the xenon dopant increases the rate of transfer to the xenon excimer state and recovers this lost light.

To use this model at low xenon concentrations (< 0.1 ppm), we can use the curve of Fig. 3 to determine the absorption factor corresponding to these low dopant levels. In this case the absorption decreases linearly

from the constant A=0.62 to zero. Thus, at these very low xenon concentrations the light yield also increases (see Fig. 13).

Finally, there has been some concern with xenon doping that particle identification using the ratio of fast to slow light would be negatively impacted. However, as seen from our model, the singlet light yield is not significantly impacted at ~ 10 ppm relative to the residual level of 0.4ppm, and while there is more light at earlier times (but after the singlet peak), it should not impact the uncertainty in the ratio of the "fast" to "slow" light, only the value of the ratio. This ratio for different primary ionization will still be determined by the relative strength of the initial singlet light, however, a tighter time window on the singlet peak will be necessary.

7. Summary and outlook

In this work we presented a model for light produced by xenon doping that accurately describes the time development of the light as measured in our experiment. The increased light yield by a factor of

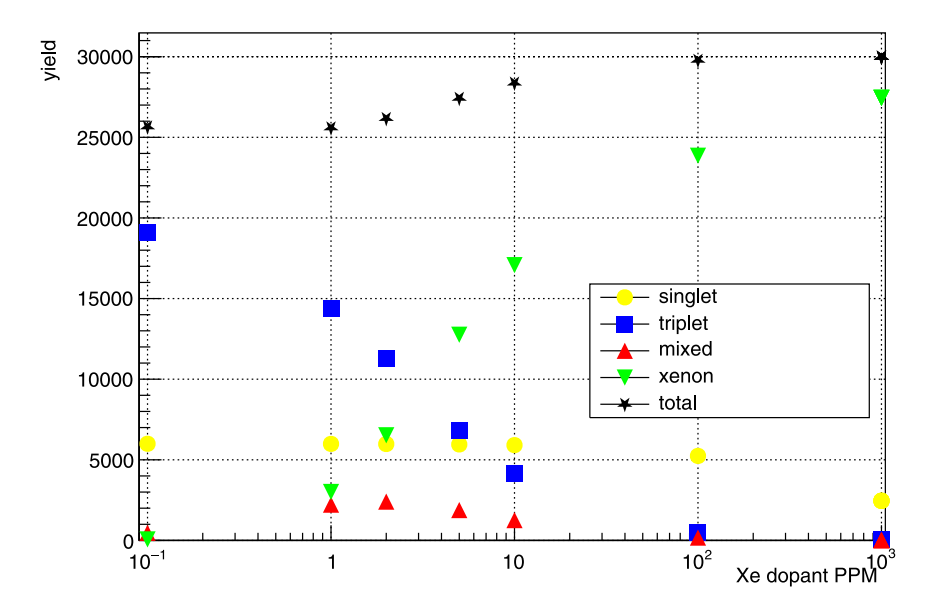


Fig. 11. Model light yield prediction with A = 0 for all xenon concentrations. We set the total number of initial excimers to be 30,000 and integrated from the trigger at 1000 ns to 10,000 ns. Markers are light from singlet (yellow dots), triplet (blue squares), mixed (red triangles), xenon (green inverted triangles) and total (black stars).

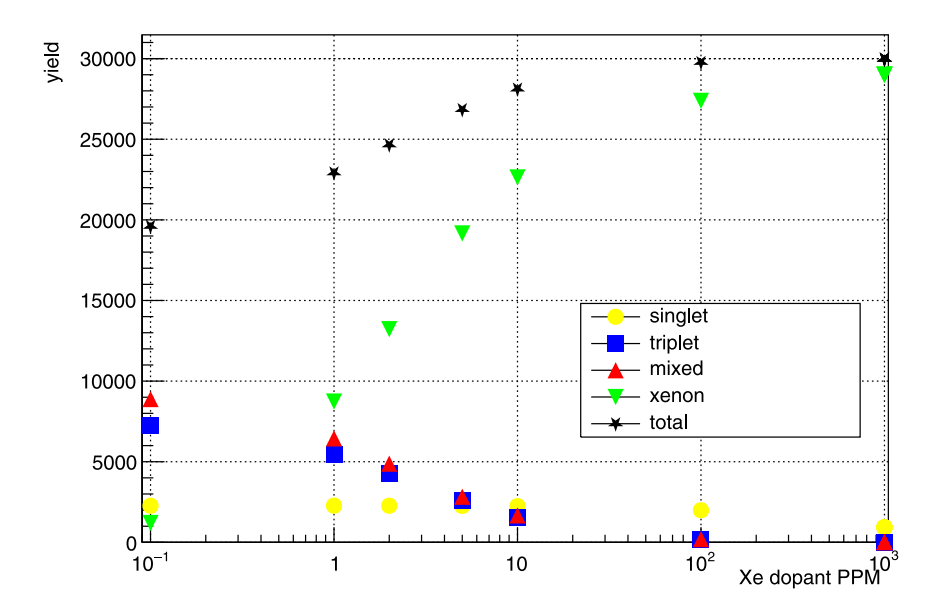


Fig. 12. Model light yield prediction with A = 0.62 kept as a constant over xenon concentrations. We set the total number of initial excimers to be 30,000 and integrated from the trigger at 1000 ns to 10,000 ns. Markers are light from singlet (yellow dots), triplet (blue squares), mixed (red triangles), xenon (green inverted triangles) and total (black stars).

 1.92 ± 0.12 at 10 ppm over the yield in argon with traces of Xenon up to a few ppm as reported in Ref. [9] is now understood as the release of the excimer trapped light with the addition of xenon. Thus, the addition of 10 ppm xenon to liquid argon detectors increases the light yield in our geometry and trigger set by a factor of two, as well as shifting the light to early times and to the more favorable 175 nm wavelength.

In future work, we will confirm our model by measuring the separate (128 and 175 nm) emission wavelengths as a function of distance and emission time. Additionally, by using a triggered source (design provided by Schönert's group at TUM [22]), by doping in finer steps below 1 ppm and by measuring the light yield accurately out to $10~\mu s$

we expect to extract values for the quenching rate and the absolute light yield in PE per deposited ionization.

Declaration of competing interest

The authors declare the following financial interests/personal relationships which may be considered as potential competing interests: Michael Gold reports equipment, drugs, or supplies was provided by Los Alamos National Laboratory.

Data availability

Data will be made available on request.

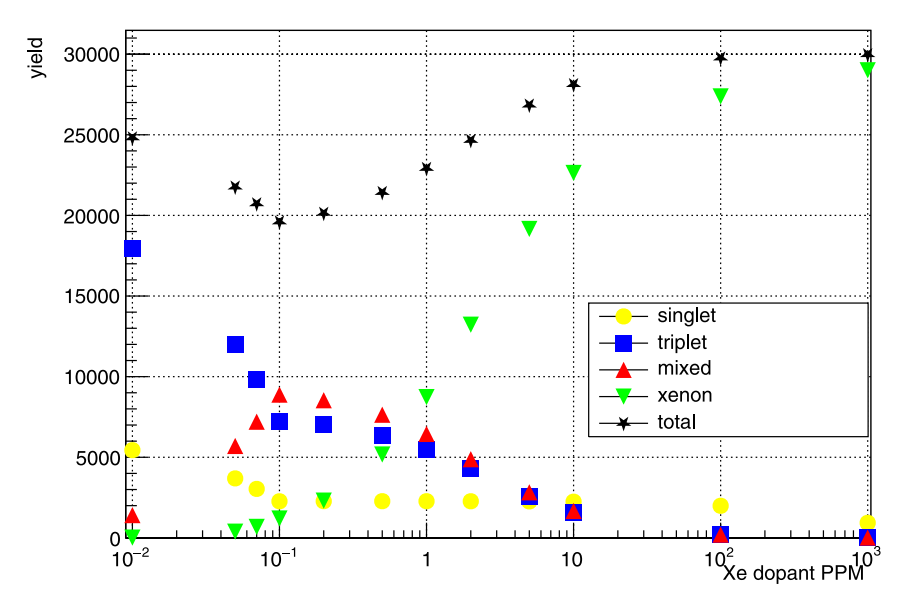


Fig. 13. Model light yield prediction with *A* taken as a function of xenon concentration based on the double exponential fit of Fig. 3. We set the total number of initial excimers to be 30,000 and integrated from the trigger at 1000 ns to 10,000 ns. Markers are light from singlet (yellow dots), triplet (blue squares), mixed (red triangles), xenon (green inverted triangles) and total (black stars).

Acknowledgments

We gratefully acknowledge the support of the U.S. Department of Energy through the LANL/LDRD Program and by the U.S. Department of Energy, Office of Science, Office of Nuclear Physics award LANL-EM78.

References

- [1] R. Ajaj, et al., DEAP Collaboration, Search for dark matter with a 231-day exposure of liquid argon using DEAP-3600 at SNOLAB, Phys. Rev. D 100 (2) (2019) 022004, http://dx.doi.org/10.1103/PhysRevD.100.022004, arXiv:1902.04048.
- [2] W.C. Louis, R.G.V. de Water, Hidden neutrino particles may be a link to the dark sector, Sci. Am. 323 (2020) 46–53, http://dx.doi.org/10.1038/ scientificamerican0720-46.
- [3] P. Agnes, et al., DarkSide-50 532-day dark matter search with low-radioactivity argon, Phys. Rev. D 98 (10) (2018) http://dx.doi.org/10.1103/physrevd.98. 102006.
- [4] D. Akimov, et al., COHERENT Collaboration, First measurement of coherent elastic neutrino-nucleus scattering on argon, Phys. Rev. Lett. 126 (2021) 012002, http://dx.doi.org/10.1103/PhysRevLett.126.012002.
- [5] M. Agostini, et al., Final results of GERDA on the search for neutrinoless double- beta decay, Phys. Rev. Lett. 125 (25) (2020) http://dx.doi.org/10.1103/ physrevlett.125.252502.
- [6] N. Abgrall, et al., LEGEND Collaboration, The large enriched germanium experiment for neutrinoless double beta decay (LEGEND), in: Proceedings, Matrix Elements for the Double Beta Decay Experiments (MEDEX'17): Prague, Czech Republic, AIP Conf. Proc. 1894 (1) (2017) 020027, http://dx.doi.org/10.1063/1.5007652, arXiv:1709.01980.
- [7] P. Peiffer, T. Pollmann, S. Schonert, A. Smolnikov, S. Vasiliev, Pulse shape analysis of scintillation signals from pure and xenon-doped liquid argon for radioactive background identification, JINST 3 (2008) P08007, http://dx.doi.org/ 10.1088/1748-0221/3/08/P08007.
- [8] A. Neumeier, T. Dandl, T. Heindl, A. Himpsl, L. Oberauer, W. Potzel, S. Roth, S. Schönert, J. Wieser, A. Ulrich, Intense vacuum ultraviolet and infrared scintillation of liquid Ar-Xe mixtures, Europhys. Lett. 109 (1) (2015) 12001, http://dx.doi.org/10.1209/0295-5075/109/12001.
- [9] N. McFadden, S. Elliott, M. Gold, D. Fields, K. Rielage, R. Massarczyk, R. Gibbons, Large-scale, precision xenon doping of liquid argon, Nucl. Instrum. Methods A 1011 (2021) 165575, arXiv:2006.09780.

- [10] A. Neumeier, T. Dandl, A. Himpsl, L. Oberauer, W. Potzel, S. Schönert, A. Ulrich, Attenuation of vacuum ultraviolet light in pure and xenon-doped liquid argon—An approach to an assignment of the near-infrared emission from the mixture, Europhys. Lett. 111 (1) (2015) 12001, http://dx.doi.org/10.1209/0295-5075/111/12001, arXiv:1511.07725.
- [11] B. Raz, J. Jortner, Experimental evidence for trapped exciton states in liquid rare gases, Proc. R. Soc. Lond. Ser. A Math. Phys. Eng. Sci. 317 (1528) (1970) 113–131.
- [12] J. Calvo, et al., Measurement of the attenuation length of argon scintillation light in the ArDM LAr TPC, Astropart. Phys. 97 (2018) 186–196, http://dx.doi.org/ 10.1016/j.astropartphys.2017.11.009.
- [13] E. Segreto, Properties of liquid argon scintillation light emission, Phys. Rev. D 103 (4) (2021) 043001, http://dx.doi.org/10.1103/PhysRevD.103.043001, arXiv: 2012.06527.
- [14] M. Kubota, S. Hishida, J. Himi, J. Suzuki, J. Ruan, The suppression of the slow component inxenon-doped liquid argon scintillation, Nucl. Instrum. Methods Phys. Res. A 327 (1993) 71–74.
- [15] J. Soto-Oton, DUNE Collaboration, Impact of xenon doping in the scintillation light in a large liquid-argon TPC, in: International Conference on Technology and Instrumentation in Particle Physics, 2021, arXiv:2109.05858.
- [16] A. Hitachi, Photon-mediated and collisional processes in liquid rare gases, NIMA 327 (1) (1993) 11–14.
- [17] C.G. Wahl, E.P. Bernard, W.H. Lippincott, J.A. Nikkel, Y. Shin, D.N. McKinsey, Pulse-shape discrimination and energy resolution of a liquid-argon scintillator with xenon doping, J. Instrum. 9 (06) (2014) P06013, http://dx.doi.org/10. 1088/1748-0221/9/06/p06013, URL https://iopscience.iop.org/article/10.1088/ 1748-0221/9/06/P06013.
- [18] G. Cini-Castagnol, Self-diffusion in liquid argon, J. Chem. Phys. 32 (19) (1960).
- [19] C. Benson, G. Orebi Gann, V. Gehman, Measurements of the intrinsic quantum efficiency and absorption length of tetraphenyl butadiene thin films in the vacuum ultraviolet regime, Eur. Phys. J. C 78 (2018) 329, http://dx.doi.org/ 10.1140/epjc/s10052-018-5807-z.
- [20] SAES, Specification Sheet. http://www.saespuregas.com/Library/documents/ s110-243 rev 528.pdf.
- [21] N. McFadden, Large-scale, precision xenon doping of liquid argon, (Thesis, University of New Mexico), 2020, https://digitalrepository.unm.edu/phyc_etds/ 220/
- [22] M. Schwarz, P. Krause, A. Leonhardt, L. Papp, S. Schönert, C.W.M.F.K. Gusev, N. Rumyantseva, E. Shevchik, D. Zinatulina, G. Araujo, Liquid argon instrumentation and monitoring in LEGEND-200, EPJ Web Conf. 253 (2021) 11014, http://dx.doi.org/10.1051/epjconf/202125311014, https://doi.org/10.1051/epjconf/202125311014.